

**RUSSIAN RESEARCH CENTER «KURCHATOV INSTITUTE»**

**DIVISION OF ADVANCED NUCLEAR POWER SYSTEMS**

APPROVE

DIRECTOR OF DIVISION

\_\_\_\_\_ P.N.Alekseev  
«\_\_»\_\_\_\_\_200 г.

**INTERCOMPARISONS OF CALCULATIONS MADE FOR RBEC-M  
FUEL CYCLE BENCHMARK**

**Status report**

Performer

\_\_\_\_\_ A.A.Dudnikov

Moscow, RRC KI

## **Contents**

### **Introduction**

#### **1. Obtained results inventory**

#### **2. Analysis of keff calculations at the beginning of the cycle**

##### **2.1. Different nuclear data libraries effect**

##### **2.2. Effects of nuclear data preprocessing**

##### **2.3. Pb data effect on the critical calculation**

#### **3. Analysis of depletion calculations during the cycle**

### **Conclusion**

### **References**

#### **Appendix 1. ANL Analysis Method**

#### **Appendix 2. BARC Analysis Method**

#### **Appendix 3. RRC KI Analysis Method**

#### **Appendix 4. TokyoTech Analysis Method**

## Introduction

The RBEC reactor facility with 900 MW(th) was proposed as fuel cycle benchmark.

Geometry of calculational model of RBEC-M reactor is shown on Fig. I1. Figures denote numbers of physical zones, differing from each other by volume fractions of materials. Axial dimensions are given in mm.

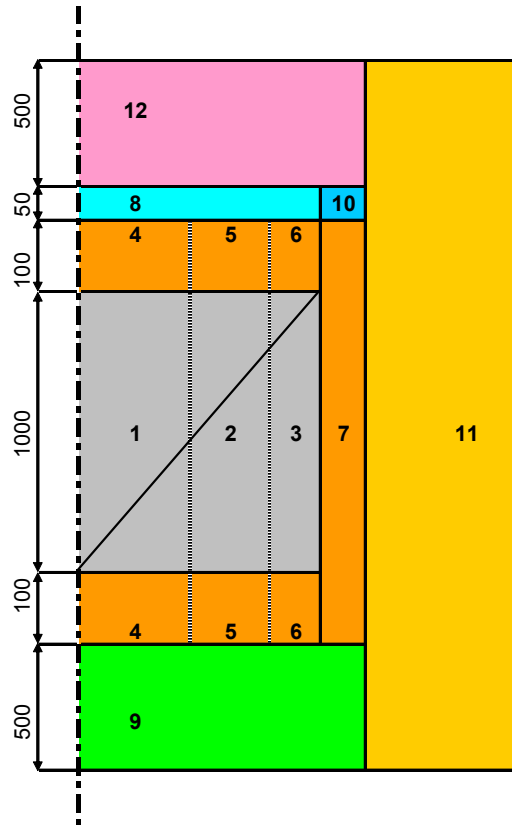


Fig. I1. Geometry of calculational model of RBEC-M reactor.

The main dimensions of physical zones are given in Table I1. The temperatures of physical zones are given in Table I2.

Table I1. Main dimensions of physical zones of RBEC-M reactor model, cm

Physical zone	#	Inner radius	Outer radius	Height
Core-1	1		86.163	100
Core-2	2	86.163	131.837	100
Core-3	3	131.837	148.652	100
Axial blanket of core-1	4		86.163	10
Axial blanket of core-2	5	86.163	131.837	10

Axial blanket of core-3	6	131.837	148.652	10
Lateral blanket	7	148.652	165.342	120
Top of fuel assemblies (FA)	8		148.652	5
Gas plenum	9		165.342	50
Top of assemblies of lateral blanket	10	148.652	165.342	5
Downcomer	11	165.342	211.262	225
Chimney	12		165.342	50

Table I2. Temperatures of physical zones of RBEC-M reactor model, K

Physical zone	#	Fuel	Steel	Coolant
Core-1	1	1200	800	700
Core-2	2	1100	800	700
Core-3	3	1000	800	700
Axial blanket of core-1	4	900/700*	800/600*	800/600*
Axial blanket of core-2	5	900/700*	800/600*	800/600*
Axial blanket of core-3	6	900/700*	800/600*	800/600*
Lateral blanket	7	700	600	600
Top of fuel assemblies (FA)	8		800	800
Gas plenum	9		600	600
Top of assemblies of lateral blanket	10		600	600
Downcomer	11		700	700
Chimney	12		800	800

\* - in top/bottom parts of physical zone

Nuclide composition of physical zones (fresh fuel) is given in Tables I3 and I4.

Fuel material -  $(U_{0.863} + Pu_{0.137})N$ . Isotopic composition of plutonium in fresh fuel corresponds to “reactor-grade” plutonium, extracted from cooled spent fuel of typical light-water reactor, while isotopic composition of uranium corresponds to depleted uranium with content of 0.1 mass%  $^{235}U$ .

Coolant materials - Pb-Bi.

Construction material - Steel (C, Si, V, Cr, Mn, Fe, Ni, Nb, Mo, W)

Table I3. Nuclear densities of components of physical zones, 1/barn·cm

Physical zone	Core-1	Core-2	Core-3	Axial blanket-1	Axial blanket-2	Axial blanket-3
#	1	2	3	4	5	6
U-235	6.42536E-06	7.61116E-06	1.05343E-05	7.47095E-06	8.84971E-06	1.22485E-05
U-238	6.35962E-03	7.53328E-03	1.04265E-02	7.36921E-03	8.72919E-03	1.20817E-02

Pu-238	1.33524E-05	1.58166E-05	2.18910E-05			
Pu-239	6.07226E-04	7.19290E-04	9.95539E-04			
Pu-240	2.43311E-04	2.88214E-04	3.98905E-04			
Pu-241	8.31945E-05	9.85480E-05	1.36396E-04			
Pu-242	4.92603E-05	5.83513E-05	8.07615E-05			
Am-241	8.08633E-06	9.57866E-06	1.32574E-05			
N-14	4.96797E-04	5.88481E-04	8.14492E-04	4.97216E-04	5.88976E-04	8.15178E-04
N-15	6.87368E-03	8.14221E-03	1.12693E-02	6.87947E-03	8.14907E-03	1.12788E-02
Bi-209	1.04654E-02	9.59466E-03	7.46809E-03	1.04654E-02	9.59466E-03	7.46809E-03
Pb-206	2.06859E-03	1.89648E-03	1.47615E-03	2.06859E-03	1.89648E-03	1.47615E-03
Pb-207	1.89696E-03	1.73913E-03	1.35367E-03	1.89696E-03	1.73913E-03	1.35367E-03
Pb-208	4.49772E-03	4.12351E-03	3.20957E-03	4.49772E-03	4.12351E-03	3.20957E-03
C	7.25829E-05	7.75886E-05	8.69743E-05	7.25829E-05	7.75886E-05	8.69743E-05
Si	2.23105E-04	2.38491E-04	2.67341E-04	2.23105E-04	2.38491E-04	2.67341E-04
V	3.74360E-05	4.00178E-05	4.48587E-05	3.74360E-05	4.00178E-05	4.48587E-05
Cr	1.15270E-03	1.23220E-03	1.38125E-03	1.15270E-03	1.23220E-03	1.38125E-03
Mn	6.44665E-05	6.89124E-05	7.72486E-05	6.44665E-05	6.89124E-05	7.72486E-05
Fe	8.22862E-03	8.79611E-03	9.86016E-03	8.22862E-03	8.79611E-03	9.86016E-03
Ni	6.03452E-05	6.45069E-05	7.23102E-05	6.03452E-05	6.45069E-05	7.23102E-05
Nb	1.75942E-05	1.88076E-05	2.10827E-05	1.75942E-05	1.88076E-05	2.10827E-05
Mo	4.25946E-05	4.55322E-05	5.10401E-05	4.25946E-05	4.55322E-05	5.10401E-05
W	1.92638E-05	2.05924E-05	2.30834E-05	1.92638E-05	2.05924E-05	2.30834E-05

Table I4. Nuclear densities of components of physical zones, 1/barn-cm

	Lateral blanket (LB)	Top of fuel assemblies	Gas Plenum	Top of LB assemblies	Downcomer	Chimney
#	7	8	9	10	11	12
U-235	1.05171E-05					
U-238	1.03738E-02					
N-14	6.99943E-04					
N-15	9.68440E-03					
Bi-209	9.46070E-03	9.52768E-03	9.52768E-03	9.46070E-03	1.50701E-02	1.66609E-02
Pb-206	1.87001E-03	1.88324E-03	1.88324E-03	1.87001E-03	2.97877E-03	3.29320E-03
Pb-207	1.71485E-03	1.72699E-03	1.72699E-03	1.71485E-03	2.73162E-03	3.01995E-03
Pb-208	4.06593E-03	4.09472E-03	4.09472E-03	4.06593E-03	6.47671E-03	7.16036E-03
C	5.88172E-05	7.75886E-05	2.22000E-04	5.88172E-05	6.25714E-05	3.12857E-06
Si	1.80792E-04	2.38491E-04	2.38491E-04	1.80792E-04	1.92332E-04	9.61659E-06
V	3.03361E-05	4.00178E-05	4.00178E-05	3.03361E-05	3.22724E-05	1.61362E-06
Cr	9.34084E-04	1.23220E-03	1.23220E-03	9.34084E-04	9.93706E-04	4.96853E-05
Mn	5.22401E-05	6.89124E-05	6.89124E-05	5.22401E-05	5.55745E-05	2.77873E-06
Fe	6.66802E-03	8.79611E-03	8.79611E-03	6.66802E-03	7.09364E-03	3.54682E-04
Ni	4.89004E-05	6.45069E-05	6.45069E-05	4.89004E-05	5.20217E-05	2.60109E-06
Nb	1.42574E-05	1.88076E-05	1.88076E-05	1.42574E-05	1.51674E-05	7.58370E-07
Mo	3.45163E-05	4.55322E-05	4.55322E-05	3.45163E-05	3.67195E-05	1.83598E-06
W	1.56104E-05	2.05924E-05	2.05924E-05	1.56104E-05	1.66068E-05	8.30338E-07
B-10			5.08102E-04			
B-11			6.95431E-05			

Reactor operates in open fuel cycle with the use of available reprocessed fuel of light-water reactors with low level of decay heat power.

Three different depletion problems are specified for the benchmark as follows:

- Burn-up cycle consists of 1800 effective full-power days.
- Burn-up cycle consists of 900 effective full-power days.
- Fuel cycle consists of six partial fuel cycles of 300 effective full-power days each. Reactor is shut down for refueling for 60 days. During refueling, 1/6 mass part of fuel and fission products in core and blanket zones is removed and “fresh” (i.e. at the beginning of cycles) fuel composition is added.

The pattern of data preparation for Mode.3 calculation is as follows:

- Cycle “*i*” begins with initial composition of core zones and blanket zones  $RHO1(i,n)$ , where  $RHO$  is nuclear concentration of heavy metals and fission products in zone “*n*” and cycle “*i*”;
- After 300 effective full-power days, the composition becomes  $RHO2(i,n)$ , and after 60 days of cooling the composition becomes  $RHO3(i,n)$ ;
- Initial composition for the next cycle “*i+1*” is calculated as follows:  
 $RHO1(i+1,n) = RHO3(i,n)*5/6 + RHO(0,n)*1/6$ , where  
“*i*” is cycle number, “*n*” is zone index,  
and  $RHO(0,n)$  is “fresh” (i.e. at the beginning of cycles) composition in zone “*n*”.

The reactor thermal power for depletion calculation in Modes 1, 2, and 3 is 900 MW(th).

## 1. Obtained results inventory

Participants of RBEC-M fuel cycle benchmark calculations:

ANL - Argonne National Laboratory, Argonne, Illinois, USA;  
 BARC - Bhabha Atomic Research Centre, Mumbai, India;  
 Hidropress – EDO “GIDROPRESS”, Podolsk, Moscow Region, Russia;  
 RRC KI – Russian Research Center “Kurchatov Institute”, Moscow, Russia;  
 TokyoTech - Tokyo Institute of Technology, Tokyo, Japan.

The calculations have been made using different code systems with nuclear data derived from different libraries. Both deterministic and Monte Carlo methods have been used. The aim of the intercomparison study has been to try to identify the sources of the discrepancies between the different methods and libraries.

Table 1 shows code systems and nuclear data libraries used by participants of benchmark calculations.

Table.1 Code systems and nuclear data libraries used

Participant	ANL	BARC	Gidropress	RRC KI	TokyoTech
Code system for cell calculation	MC <sup>2</sup> -2		GNDL		SRAC
Code system for criticality calculation	DIF3D, TWODANT	ERANOS2.0	DIFRZ, KINRZ	MCNP5	Original
Code system for fuel cycle analysis	REBUS-3		BURNUPRZD, BURNUPRZK	ISTAR-2	Original
Nuclear data library	ENDF/B-V.2	JEF2	ENDF/B-VI.3, ENDF/B-VI.5	ENDF/B-VI.8 (main)	JENDL3.3
Number of energy groups	33, 230	33	30	Pointwise cross-section data	21

It should be pointed that all participants have used evaluated nuclear data libraries ENDF/B-V/VI, JEF2 or JENDL3.3 (pointwise cross-section data) as data source, but then most of participants have performed multigroup criticality calculations during campaign. Multigroup libraries usually contain several combined fission products – this option reduces drastically number of fission products in criticality calculation, but can produce some additional error especially for new type of reactor and neutron spectra. The other way chosen by RRC KI is taking in account fission products as it is – about 100 in criticality calculations and about 1000 in isotope kinetics, but it makes calculations more complicated and needs significantly more time.

Table.2 and Figure.1 shows the evolution of multiplication factor  $k_{\text{eff}}$  on 1800-day campaign at thermal power 900 MW.

Table.2 Evolution of keff on 1800-day campaign at thermal power 900 MW

Participant	ANL		BARC	Gidropress		RRC KI	TokyoTech
	DIF3D	TWODANT	ERANOS2.0	DIFRZ	KINRZ	MCNP5	Original
0	0.99721	0.99777	0.99498	1.0076	1.0084	1.00383	1.00271
100	1.00011	1.00063	0.99544	1.0077	1.0085		1.00261
200	1.00284	1.00333	0.99671	1.0086	1.0094		1.00322
300	1.00539	1.00586	0.99785	1.0093	1.0102		1.00374

400	1.00778	1.00822	0.99887	1.0100	1.0109		1.00418
500	1.00999	1.01042	0.99977	1.0106	1.0114		1.00453
600	1.01203	1.01246	1.00054	1.0110	1.0120		1.00479
700	1.01392	1.01435	1.00121	1.0114	1.0124		1.00497
800	1.01565	1.01608	1.00176	1.0117	1.0127		1.00505
900	1.01724	1.01767	1.00221	1.0119	1.0128	1.01224	1.00505
1000	1.01934	1.01912	1.00254	1.0120	1.0131		1.00497
1200	1.02183	1.02162	1.00292	1.0120	1.0132		1.00457
1400	1.02382	1.02363	1.00292	1.0117	1.0128		1.00387
1600	1.02535	1.02519	1.00258	1.0111	1.0122		1.00289
1800	1.02647	1.02635	1.00192	1.0102	1.0113	1.01024	1.00166

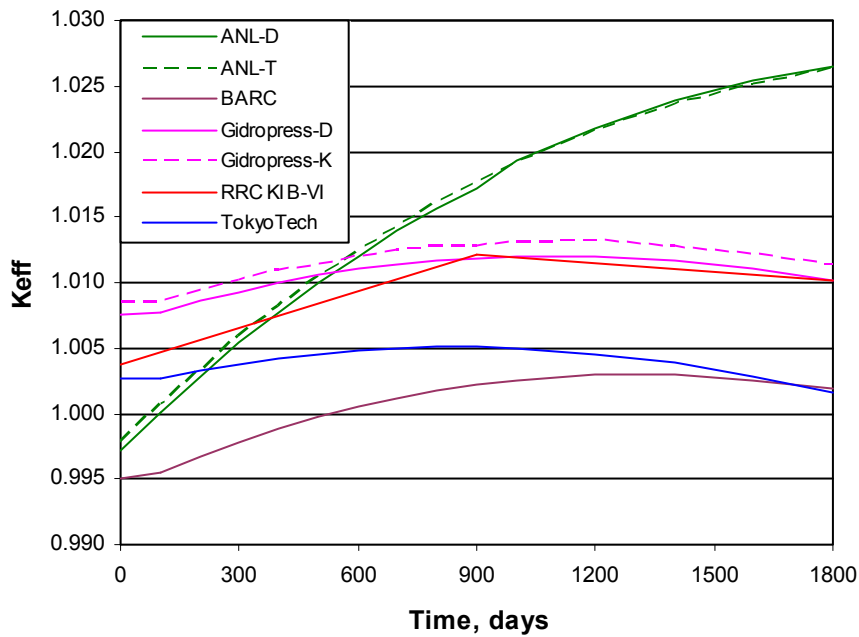


Figure.1 Evolution of  $k_{eff}$  on 1800-day campaign at thermal power 900 MW

Figure.1 shows two sorts of  $k_{eff}$  evolution – steady increase (ANL) and little increase in the first half of campaign and little decrease to the end (BARC, Gidropress, RRC KI, TokyoTech). Largest discrepancies occur at the beginning of the campaign between BARC and Gidropress calculations: 1342 pcm, and at the end of the campaign between ANL and BARC calculations: 2443 pcm.

Burnup calculations presented by ANL and Gidropress were performed using different methods (neutron diffusion and neutron transport theory) but with the same nuclear data evaluation. Results show that discrepancies in  $k_{eff}$  rather have source in nuclear data.

Table.3 Region powers, Watts

Time, days	Zone	ANL	BARC	Gidropress	RRC KI	TokyoTech
0	Core1	3.31E+08	3.39E+08	3.39E+08	3.42E+08	3.49E+08
	Core2	3.97E+08	3.95E+08	3.92E+08	3.98E+08	3.99E+08
	Core3	1.50E+08	1.45E+08	1.45E+08	1.48E+08	1.40E+08
900	Core1	3.34E+08	3.35E+08	3.33E+08	3.39E+08	3.42E+08

	Core2	3.77E+08	3.79E+08	3.78E+08	3.79E+08	3.83E+08
	Core3	1.40E+08	1.41E+08	1.41E+08	1.42E+08	1.36E+08
1800	Core1	3.23E+08	3.20E+08	3.19E+08	3.20E+08	3.25E+08
	Core2	3.67E+08	3.70E+08	3.69E+08	3.72E+08	3.75E+08
	Core3	1.39E+08	1.42E+08	1.42E+08	1.44E+08	1.38E+08

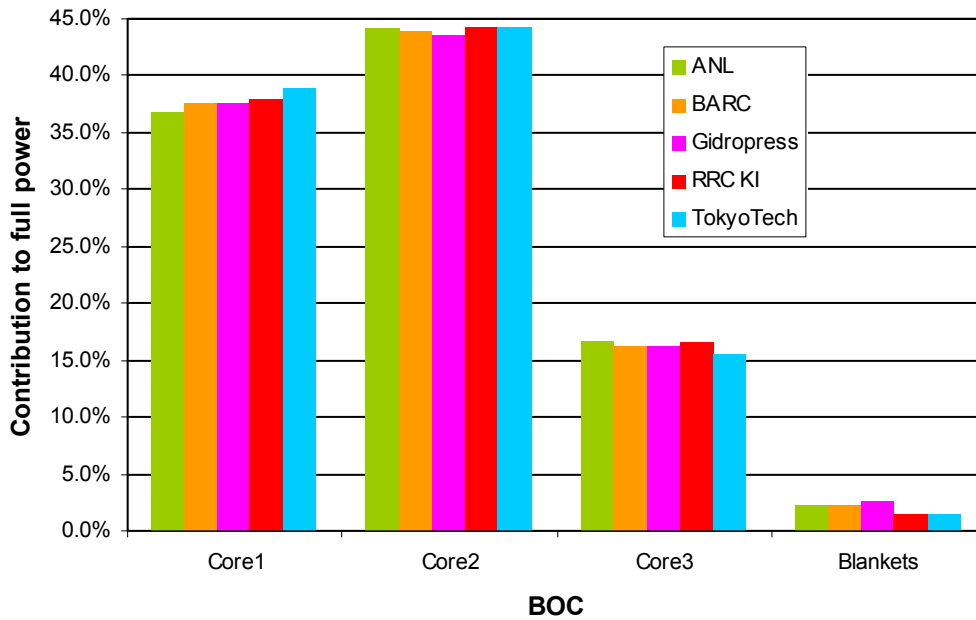


Figure.2 Region powers at the beginning of the cycle

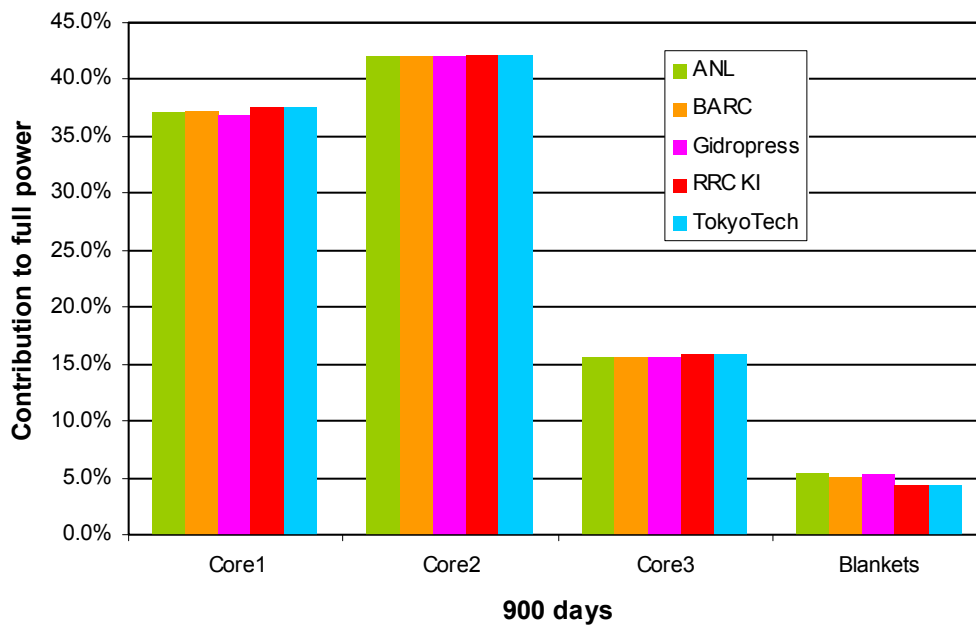


Figure.3 Region powers at 900 days

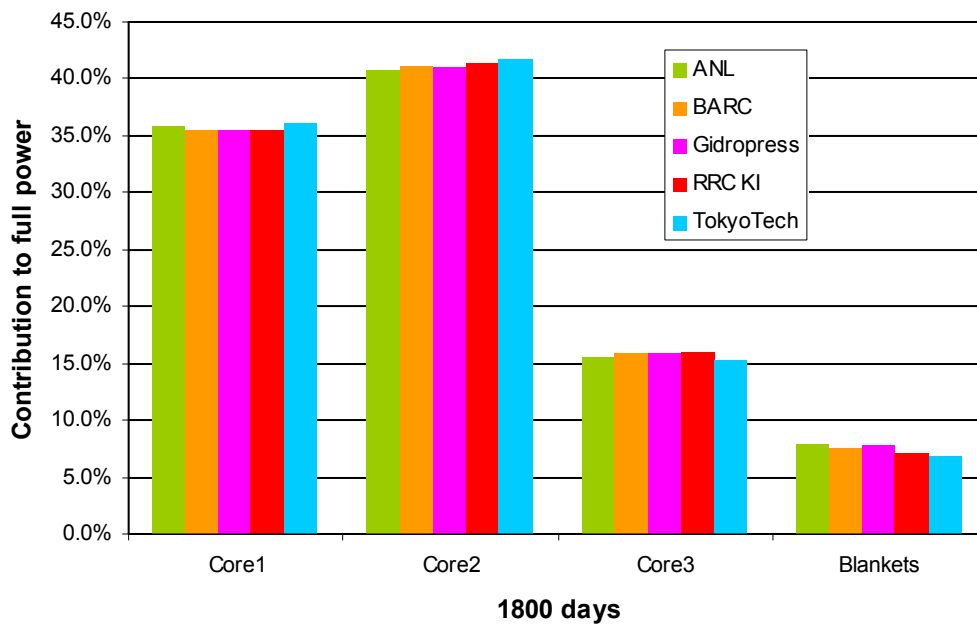


Figure.4 Region powers at 1800 days

## 2. Analysis of keff calculations at the beginning of the cycle

Discrepancies in keff at the start point of the cycle (Table 4) when fission products are absent, can have its origins in methods, codes and nuclear data libraries. Nowadays for the fast reactor criticality calculations both methods and well known engineering codes produce very close results (and the good examples are ANL and Gidropress calculations using diffusion and transport theory).

Table.4 keff at the beginning of the cycle

Participant	Code	Nuclear data	keff	keff <sup>CODE</sup> – keff <sup>RRC KI</sup> , pcm
ANL	TWODANT	ENDF/B-V.2	0.99777	-606
BARC	ERANOS2.0	JEF2	0.99498	-885
Gidropress	KINRZ	ENDF/B-VI	1.0084	457
RRC KI	MCNP5	ENDF/B-VI	1.00383	-
TokyoTech	Original	JENDL-3.3	1.00271	-112

So, nuclear data libraries and data preprocessing should be the cause of k<sub>eff</sub> discrepancies.

### 2.1. Different nuclear data libraries effect

To clarify the effect of different libraries additional criticality calculations of Core1 infinite medium at the beginning of the cycle were performed and neutron balances were obtained using MCNP5 and nuclear data from ENDF/B-V (release 2), ENDF/B-VI, JEF-3.1 and JENDL-3.3 libraries. Results are shown in Table 5.

Table.5 Neutron balance in Core1 infinite medium at BOL

	ENDF/B-V			ENDF/B-VI			JEF-3.1			JENDL-3.3		
Kinf	1.1535			1.1660			1.1663			1.1471		
Nuclide	Capt.	Fiss.	Gen.	Capt.	Fiss.	Gen.	Capt.	Fiss.	Gen.	Capt.	Fiss.	Gen.
U-235	2	7	18	2	7	18	2	8	19	2	8	19
U-238	<b>1124</b>	118	290	<b>1105</b>	117	<b>294</b>	1111	111	273	<b>1132</b>	112	<b>281</b>
Pu-238	6	9	27	6	9	28	4	10	30	5	9	26
Pu-239	162	677	1983	164	675	1984	169	678	1990	<b>179</b>	682	<b>2002</b>
Pu-240	73	54	156	71	55	157	69	54	158	78	51	145
Pu-241	22	125	372	21	128	379	24	130	388	24	131	391
Pu-242	12	8	22	13	8	22	14	8	22	14	7	20
Am-241	8	1	4	8	1	4	9	1	4	9	1	4
FP												
Struct.	<b>78*</b>			69			67			69**		
Coolant	46*			49			43			<b>37</b>		
Total	1532	1000	2872	1509	1000	2886	1512	1000	2883	1550	1000	2887

\*) for Am-241, Bi-209, Ni, Nb-93 and W we could not obtain ENDF/B-V data and have used information from ENDF/B-VI.

\*\*) for Nb-93 we could not obtain JENDL-3.3 data and have used information from ENDF/B-VI.

In this table Capt. denotes Capture, Fiss. – Fission, Gen. – Generation, FP – Fission products, Struct. – Structure isotopes, Coolant – Coolant isotopes.

The discrepancies in neutron multiplication factor (kinf) due to using various nuclear data libraries for Core1 infinite medium at BOL are shown in Table 6.

Table.6 Neutron multiplication factor kinf for Core1 infinite medium at BOL

Nuclear data library	ENDF/B-V	ENDF/B-VI	JEF-3.1	JENDL-3.3
kinf	1.1535	1.1660	1.1663	1.1471
$(\text{kinf}^{\text{LIBR}} - \text{kinf}^{\text{B-VI}})$ , pcm	-1250	-	30	-1890

From Table 6 one can see that neutron multiplication factor depends on data library used and discrepancy can be more than 1800 pcm. Neutron balances in Table 5 are useful to illustrate these discrepancy origins:

- ENDF/B-V in comparison with ENDF/B-VI:

Neutron balance components for heavy isotopes are practically the same excluding U-238. Neutron capture by U-238 from B-V is larger than by U-238 from B-VI and neutron generation is smaller. In structure isotopes neutron capture by Cr and Mo is larger (by +6 and +4 correspondingly) than for B-VI. These factors reduce kinf. In coolant neutron capture by Pb is smaller (-3) than for B-VI.

- JEF-3.1 in comparison with ENDF/B-VI:

Neutron balance components differ slightly from components produced by ENDF/B-VI, but total parameters are practically the same. Therefore neutron multiplication factors are close. Neutron capture in coolant by Bi and Pb is smaller (by -4 and -2 correspondingly) than for B-VI.

- JENDL-3.3 in comparison with ENDF/B-VI:

Smaller neutron generation by U-238 and Pu-240 and larger generation by Pu-239 and Pu-241 results in practically the same total generation. But larger capture by heavy nuclides, especially U-238 and Pu-239, results in significantly large total capture and drastically reduces kinf. Neutron capture in coolant by Bi and Pb is smaller (by -7 and -5 correspondingly) than for B-VI.

## 2.2. Effects of nuclear data preprocessing

A multigroup approach used by most of participants also is the source of the discrepancies. To generate correct multigroup cross section library on the base of chosen neutron data library it is important to select correct energy group structure and neutron spectra for physical zones of problem solving. Usually it is necessary to do some iteration for neutron spectra correction. Using standard multigroup libraries can produce additional discrepancies when standard neutron spectra differ from spectra in problem zones especially for new types of reactors.

Table 7 shows neutron balances in Core1 infinite medium at BOL calculated by MCNP5 using ENDF/B-VI and ENDF/B-V libraries and calculated in ANL using multigroup cross section data generated for each homogenized zone in the benchmark [Appendix 1]. 33-group and 230-group cross section structures were implemented for the specified composition and component-wise temperatures using the MC<sup>2</sup>-2 code. ENDF/B-V.2 data was used for all isotopes. For the three core zones, a critical buckling calculation

was used with a consistent  $P_1$  approximation and the corresponding spectrum was used for group collapsing. For the remaining compositions, a fixed source, derived from the leakage spectrum from an adjacent zone, was used to determine the collapsing spectrum. As an example, the leakage spectrum from the core zone was used as a fixed source in the adjoining blanket region to obtain a new collapsing spectrum. The leakage spectrum derived from the blanket calculation was then used as a fixed source in the fission gas plenum. This process is replicated for all other regions progressing the leakage from the core through all adjoining regions in the domain.

Table.7 Neutron balance in Core1 infinite medium at BOL (ANL contribution)

	ENDF/B-VI			ENDF/B-V			ANL		
Kinf	1.1660			1.1535			1.1527		
Nuclide	Capt.	Fiss.	Gen.	Capt.	Fiss.	Gen.	Capt.	Fiss.	Gen.
U-235	2	7	18	2	7	18	2	7	18
U-238	1105	117	294	1124	118	290	<b>1106</b>	119	<b>326</b>
Pu-238	6	9	28	6	9	27	6	9	28
Pu-239	164	675	1984	162	677	1983	161	677	1983
Pu-240	71	55	157	73	54	156	73	55	<b>163</b>
Pu-241	21	128	379	22	125	372	22	125	370
Pu-242	13	8	22	12	8	22	12	8	23
Am-241	8	1	4	8	1	4	8		4
FP									
Struct.	69			78			78		
Coolant	49			46			<b>66</b>		
Total	1509	1000	2886	1532	1000	2872	1533	1000	2916

ANL calculation in comparison with MCNP5 & ENDF/B-V:

Neutron balance components for heavy isotopes are practically the same excluding U-238 and Pu-240. Neutron capture by U-238 from ANL calculation is smaller than for U-238 from B-V and neutron generation is larger because of total fission neutron production in ANL calculation equals 2.74 and in B-V calculation equals 2.46. Neutron generation by Pu-240 is also larger in ANL calculation because of total fission neutron production in ANL calculation equals 2.96 and in B-V calculation equals 2.89. Neutron capture by coolant in ANL calculation is by 20 units larger than in B-V calculation and practically compensates smaller capture by U-238. In ANL calculation total neutron capture is the same as in MCNP5 & B-V calculation, total neutron generation is significantly larger, but kinf is smaller and this fact requires additional explanation.

Table 8 shows neutron balances in Core1 infinite medium at BOL calculated by MCNP5 using ENDF/B-VI and JEF-3.1 libraries and calculated in BARC using JEF2 based multigroup nuclear data libraries supplied with the code package ERANOS2.0 [Appendix 2].

BARC calculation in comparison with MCNP5 & JEF-3.1:

Practically all neutron balance components for heavy isotopes in BARC calculation differ from JEF-3.1 calculation. Neutron generation by U-238 and Pu-239 is more large in BARC calculation (+27 and +13 correspondingly) because of total fission neutron production in BARC calculation equals 2.74 and in JEF-3.1 calculation equals

2.46, and by Pu-240 and Pu-241 – smaller (-4 and -15 correspondingly). Neutron capture by U-238, Pu-239 and coolant also is larger in BARC calculation (+5, +11 and +23 correspondingly). Total balances differ significantly. Using multigroup nuclear data library preprocessed for problems with neutron spectra different (softer) from benchmark may be the reason.

Table.8 Neutron balance in Core1 infinite medium at BOL (BARC contribution)

Kinf	ENDF/B-VI			JEF-3.1			BARC		
	1.1660			1.1663					
Nuclide	Capt.	Fiss.	Gen.	Capt.	Fiss.	Gen.	Capt.	Fiss.	Gen.
U-235	2	7	18	2	8	19	2	7	18
U-238	1105	117	294	1111	111	273	1116	117	<b>320</b>
Pu-238	6	9	28	4	10	30	4	9	28
Pu-239	164	675	1984	169	678	1990	<b>180</b>	682	<b>2003</b>
Pu-240	71	55	157	69	54	158	73	51	154
Pu-241	21	128	379	24	130	388	23	126	373
Pu-242	13	8	22	14	8	22	12	7	21
Am-241	8	1	4	9	1	4	10	1	4
FP									
Struct.	69			67			69		
Coolant	49			43			<b>66</b>		
Total	1509	1000	2886	1512	1000	2883	1555	1000	2921

Table 9 shows neutron balances in Core1 infinite medium at BOL calculated by MCNP5 using ENDF/B-VI and JENDL-3.3 libraries and calculated in TokyoTech. Microscopic cross sections of each nuclide and energy groups was calculated by SRAC code system that is produced by JAEA (Japan Atomic Energy Agency). In this system, JENDL-3.3 is used as nuclear data set [Appendix 4].

Table.9 Neutron balance in Core1 infinite medium at BOL (TokyoTech contribution)

Kinf	ENDF/B-VI			JENDL-3.3			TokyoTech		
	1.1660			1.1471					
Nuclide	Capt.	Fiss.	Gen.	Capt.	Fiss.	Gen.	Capt.	Fiss.	Gen.
U-235	2	7	18	2	8	19	2	8	20
U-238	1105	117	294	1132	112	281	<b>1158</b>	<b>134</b>	<b>362</b>
Pu-238	6	9	28	5	9	26	4	10	26
Pu-239	164	675	1984	179	682	2002	<b>168</b>	<b>662</b>	<b>1948</b>
Pu-240	71	55	157	78	51	145	<b>72</b>	54	<b>162</b>
Pu-241	21	128	379	24	131	391	22	<b>124</b>	<b>370</b>
Pu-242	13	8	22	14	7	20	12	8	24
Am-241	8	1	4	9	1	4	10	0	4
FP									
Struct.	69			69			<b>139</b>		
Coolant	49			37					
Total	1509	1000	2886	1550	1000	2887	<b>1587</b>	1000	<b>2916</b>

TokyoTech calculation in comparison with MCNP5 & JENDL-3.3:

Practically all neutron balance components for heavy isotopes in TokyoTech calculation differ significantly from JENDL-3.3 calculation. For U-238 total fission neutron production in TokyoTech calculation equals 2.70 and in JENDL-3.3 calculation equals 2.51. Total balances are larger in TokyoTech calculation. Using neutron spectra different (softer) from benchmark for multigroup microscopic cross sections calculation may be the reason.

Table 10 shows neutron balances in Core1 infinite medium at BOL calculated by MCNP5 using RUSFOND [1] and ENDF/B-VII libraries.

Table.10 Neutron balance in Core1 infinite medium at BOL (additional data)

	ENDF/B-VI			RUSFOND			ENDF/B-VII		
Kinf	1.1660			1.1645			1.1559		
Nuclide	Capt.	Fiss.	Gen.	Capt.	Fiss.	Gen.	Capt.	Fiss.	Gen.
U-235	2	7	18	2	8	19	2	8	19
U-238	1105	117	294	1112	115	276	1118	114	287
Pu-238	6	9	28	5	9	27	6	9	27
Pu-239	164	675	1984	171	677	1987	168	678	1991
Pu-240	71	55	157	74	53	151	73	53	153
Pu-241	21	128	379	17	130	394	22	129	383
Pu-242	13	8	22	14	7	20	13	7	21
Am-241	8	1	4	9	1	4	9	1	4
FP									
Struct.	69			68			70		
Coolant	49			48			48		
Total	1509	1000	2886	1521	1000	2877	1529	1000	2884

RUSFOND library was distributed in 2006-2007 and contains evaluated nuclear data files for 653 nuclides. Files contain combinations of new evaluations and revised data mainly from ENDF/B-VII, JEF-3.1 and JENDL-3.3. For Core1 infinite medium at BOL neutron multiplication factor kinf from RUSFOND calculation is close to kinf from ENDF/B-VI calculation. Difference between kinf from ENDF/B-VII calculation and from ENDF/B-VI calculation is about -1000 pcm.

### 2.3. Pb data effect on the critical calculation

Reaction rates for the sum of Pb isotopes in a given group structure received from participants are shown in Table 11.

Table.11 Pb neutron reaction rates in 4-group structure

ANL*	Mode 1, BOL	
Top Energy, MeV	$\Sigma$ -total, 1/cm	$\Sigma$ -removal, 1/cm
10	5.51E-03	5.94E-04
0.835	2.81E-02	5.77E-04
0.115	3.39E-02	7.15E-04
0.009586	5.93E-03	9.61E-05
Total	7.34E-02	1.98E-03

BARC		Mode 1, BOL	
Top Energy, MeV	$\Sigma$ transport, 1/cm	$\Sigma$ removal, 1/cm	
10	3.70E-02	2.71E-03	
0.821	5.63E-02	4.33E-04	
0.111	9.38E-02	1.95E-04	
0.009118	9.52E-02	0	
Total	2.82E-01	3.34E-03	
TokyoTech		Mode 1, BOL	
Top Energy, MeV	$\Sigma$ transport, 1/cm	$\Sigma$ removal, 1/cm	
10	5.73E-02	6.56E-03	
0.821	8.38E-02	7.27E-04	
0.111	1.41E-01	1.51E-04	
0.009118	1.48E-01	9.18E-16	
Total	4.31E-01	7.44E-03	

\*) Reaction rates were received in 33-group structure and were converted to 4-group structure using neutron spectrum in Core1 infinite medium from B-V calculation.

It should be noted that transport and removal cross section definition depends on type of neutron transport problem solved, so it is difficult to compare this data. For this purpose MCNP calculations were performed and results are shown in Table 12.

Table.12 Pb neutron reaction rates component from MCNP5 calculation

		$\Sigma$ total, 1/cm			
Top E, MeV	ENDF/B-V	ENDF/B-VI	JEF-3.1	JENDL-3.3	
10	5.52E-03	5.46E-03	4.93E-03	5.09E-03	
0.821	2.83E-02	2.82E-02	2.86E-02	2.88E-02	
0.111	3.39E-02	3.28E-02	3.41E-02	3.30E-02	
0.009118	5.93E-03	6.19E-03	6.65E-03	6.11E-03	
Total	7.37E-02	7.27E-02	7.43E-02	7.29E-02	
		$\Sigma$ elastic, 1/cm			
Top E, MeV	ENDF/B-V	ENDF/B-VI	JEF-3.1	JENDL-3.3	
10	5.01E-03	4.94E-03	4.34E-03	4.60E-03	
0.821	2.83E-02	2.82E-02	2.85E-02	2.87E-02	
0.111	3.39E-02	3.28E-02	3.41E-02	3.29E-02	
0.009118	5.93E-03	6.19E-03	6.65E-03	6.10E-03	
Total	7.31E-02	7.21E-02	7.36E-02	7.24E-02	
		$\Sigma$ inelastic, 1/cm			
Top E, MeV	ENDF/B-V	ENDF/B-VI	JEF-3.1	JENDL-3.3	
10	5.04E-04	5.20E-04	5.89E-04	4.91E-04	
0.821	2.32E-05	2.76E-05	3.19E-05	2.38E-05	
0.111	0	0	0	0	
0.009118	0	0	0	0	
Total	5.27E-04	5.48E-04	6.21E-04	5.15E-04	
		$\Sigma$ absorption, 1/cm			
Top E, MeV	ENDF/B-V	ENDF/B-VI	JEF-3.1	JENDL-3.3	
10	2.06E-06	2.74E-06	2.36E-06	9.66E-07	
0.821	1.62E-05	1.64E-05	9.50E-06	1.52E-05	
0.111	1.27E-05	1.47E-05	1.45E-05	1.49E-05	
0.009118	2.85E-06	3.85E-06	4.09E-06	3.82E-06	
Total	3.38E-05	3.76E-05	3.05E-05	3.49E-05	

Total neutron capture by Pb in these calculations is maximal for B-VI, less for B-V and minimal for JEF-3.1. It corresponds with data in Table 5, taking into account that for JENDL-3.3 neutron capture by Bi-209 is also less than for other libraries.

Inelastic cross section is responsible for neutrons removal under threshold of U-238 fission reaction. Maximal contribution of this reaction gives inelastic cross section in energy range 1.4 – 6.5 MeV. A number of works consider effects of uncertainties in Pb cross section data for lead-cooled benchmarks [2, 3].

In RBEC-M benchmark homogeneous composition nuclear density of U-238 is about 75% of Pb nuclear density but  $\Sigma$  inelastic for U-238 in range 10 – 0.821 MeV is more than 3 times larger than for Pb (see Table 13).

Table.13 U-238  $\Sigma$  inelastic for Core1 infinite medium, 1/cm

U-238	$\Sigma$ inelastic, 1/cm				
Top E, MeV	ENDF/B-V	ENDF/B-VI	JEF-3.1	JENDL-3.3	ENDF/B-VII
10	1.97E-03	1.93E-03	1.91E-03	1.81E-03	1.86E-03
0.821	4.10E-03	3.90E-03	3.24E-03	3.54E-03	3.90E-03
0.111	3.12E-04	3.47E-04	2.95E-04	3.27E-04	3.40E-04
0.009118	0	0	0	0	0
Total	6.39E-03	6.18E-03	5.44E-03	5.67E-03	6.11E-03

To try to understand the effect of inelastic cross section uncertainties on the benchmark reactivity it is necessary to consider sum of  $\Sigma$  inelastic for U-238 and Pb. Figure 5 shows the result.

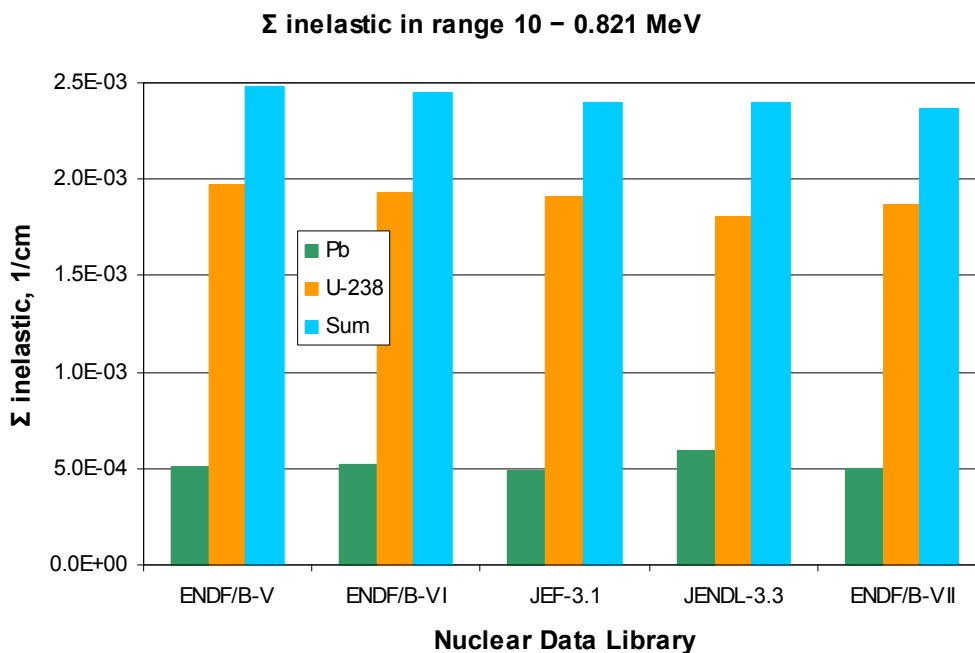


Figure.5  $\Sigma$  inelastic of U-238 and Pb for the set of nuclear data libraries

Variations in sum of  $\Sigma$  inelastic do not correlate with the variation of  $k_{inf}$  (see Table 6). So at this stage of investigations we cannot define the effect of Pb inelastic cross section uncertainties on the benchmark reactivity.

### 3. Analysis of depletion calculations during the cycle

An important requirement of correct depletion calculation is correct calculation of region power during the cycle. Region powers for begin of life, 900 effective full power days (EFPD) burning and end of life (1800 EFPD) are shown on Table 3 and Figures 2, 3 and 4. Table 14 shows region power variations weighted by region contribution to full power.

Table.14 Region power variations during the cycle

Time, days	Zone	ANL	BARC	Gidropress	RRC KI	TokyoTech
0	Core1	-1.2%	-0.3%	-0.3%	–	0.8%
	Core2	-0.1%	-0.3%	-0.7%	–	0.1%
	Core3	0.2%	-0.3%	-0.3%	–	-0.8%
900	Core1	-0.5%	-0.4%	-0.7%	–	0.3%
	Core2	-0.2%	0.0%	-0.1%	–	0.4%
	Core3	-0.2%	-0.1%	-0.1%	–	-0.6%
1800	Core1	0.3%	0.0%	-0.1%	–	0.6%
	Core2	-0.5%	-0.2%	-0.3%	–	0.3%
	Core3	-0.5%	-0.2%	-0.2%	–	-0.6%

For all variants (excluding Core1 at BOL in ANL calculation) power variations are less than 1%, and generally less than 0.5%. So all participants can calculate correct region power distribution. Figure 1 shows the similar types of evolution  $k_{eff}$  on 1800-day campaign in BARC, Gidropress, RRC KI and TokyoTech simulations – slight increase due to breeding in blankets and then decrease due to fission products accumulation. Tables 15, 16, 17 and 18 show evolution of neutron balances in infinite medium with composition of reactor Core1 at three points of cycle: BOL, Mid point and EOL.

Table.15 Neutron balance in infinite medium with reactor Core1 composition (BARC)

BARC Kinf	BOL			Mid point (900 days)			EOL (1800 days)		
	Capt.	Fiss.	Gen.	Capt.	Fiss.	Gen.	Capt.	Fiss.	Gen.
U-235	2	7	18	1	5	11	1	3	7
U-238	1116	117	320	1027	110	303	968	105	289
Pu-238	4	9	28	4	8	23	3	8	22
Pu-239	180	682	2003	188	725	2132	191	743	2185
Pu-240	73	51	154	76	55	164	80	59	176
Pu-241	23	126	373	16	87	258	13	70	209
Pu-242	12	7	21	12	7	21	12	7	21
Other h. i.	10	1	4	17	3	11	21	5	16
FP				85			166		
Struct.	69			68			68		
Coolant	66			65			65		
Total	1555	1000	2921	1559	1000	2923	1588	1000	2925

In BARC simulation one can see burnup of U-235, U-238, Pu-238 and Pu-241, generation of Pu-239, Pu-240 and other heavy isotopes, and accumulation of fission products. Pu-239 generation grows during the cycle, so core breeding ratio is greater than 1.

Table.16 Neutron balance in infinite medium with reactor Core1 composition (RRC KI)

RRC KI	BOL			Mid point (900 days)			EOL (1800 days)		
Kinf	1.1660			1.1649			1.1517		
Nuclide	Capt.	Fiss.	Gen.	Capt.	Fiss.	Gen.	Capt.	Fiss.	Gen.
U-235	2	7	18	1	5	11	1	5	11
U-238	1105	117	294	1012	110	277	1007	111	280
Pu-238	6	9	28	4	7	21	4	7	21
Pu-239	164	675	1984	172	722	2122	170	721	2120
Pu-240	71	55	157	72	58	164	72	58	165
Pu-241	21	128	379	14	87	258	14	86	257
Pu-242	13	8	22	12	7	21	12	8	22
Other h. i.	8	1	4	18	4	14	18	4	14
FP				90			170		
Struct.	69			68			68		
Coolant	49			48			48		
Total	1509	1000	2886	1511	1000	2890	1584	1000	2890

In RRC KI simulation one can see stabilization of neutron balances (excluding fission products accumulation) during the second half of the cycle. It is correct because of RBEC-M benchmark was created on the base of project of reactor with core breeding ratio close to 1.

Table.17 Neutron balance in infinite medium with reactor Core1 composition (TokyoTech)

TokyoTech	BOL			Mid point (900 days)			EOL (1800 days)		
Kinf									
Nuclide	Capt.	Fiss.	Gen.	Capt.	Fiss.	Gen.	Capt.	Fiss.	Gen.
U-235	2	8	20	2	4	12	0	4	8
U-238	1158	134	362	1038	124	337	960	118	319
Pu-238	4	10	26	4	8	22	4	8	22
Pu-239	168	662	1948	178	711	2094	182	731	2154
Pu-240	72	54	162	74	58	170	78	60	180
Pu-241	22	124	370	16	84	248	12	68	202
Pu-242	12	8	24	12	8	24	12	8	22
Other h. i.	10	0	4	16	4	12	22	4	16
FP				90			172		
Struct.	139			134			133		
Coolant									
Total	1587	1000	2916	1563	1000	2918	1574	1000	2922

In TokyoTech simulation one can see burnup of U-235, U-238 and Pu-241, generation of Pu-239, Pu-240 and slightly other heavy isotopes, and accumulation of fission products.

As in BARC simulation the growing of Pu-239 generation shows that core breeding ratio is greater than 1.

Table.18 Neutron balance in infinite medium with reactor Core1 composition (ANL)

ANL	BOL			Mid point (900 days)			EOL (1800 days)		
Kinf	1.1527			1.1719			1.1755		
Nuclide	Capt.	Fiss.	Gen.	Capt.	Fiss.	Gen.	Capt.	Fiss.	Gen.
U-235	2	7	18	1	5	11	1	3	7
U-238	1106	119	326	1014	112	305	956	106	289
Pu-238	6	9	28	4	7	22	4	7	20
Pu-239	161	677	1983	170	723	2119	175	744	2180
Pu-240	73	55	163	74	57	168	77	59	176
Pu-241	22	125	370	15	87	258	12	70	209
Pu-242	12	8	23	12	8	23	11	7	22
Other h. i.	8		4	15	3	9	19	3	11
FP				44			88		
Struct.	78			76			77		
Coolant	66			65			65		
Total	1533	1000	2916	1492	1000	2914	1485	1000	2916

ANL simulation, however, presents  $k_{eff}$  growing during the cycle. Table 18 shows that neutron capture by fission products is about half of value of this component in other simulations. In addition, the growing of Pu-239 generation shows that core breeding ratio is greater than 1.

Table.19 Heavy isotope nuclear density evolution during the cycle, 1/barn·cm

ANL	Core1			Lateral blanket		
Isotope	BOL	Mid Point	EOL	BOL	Mid Point	EOL
U-238	6.360E-03	9.926E-03	9.340E-03	1.037E-02	1.698E-02	1.674E-02
Pu-239	6.072E-04	1.099E-03	1.127E-03		2.210E-04	4.117E-04
Pu-240	2.433E-04	4.207E-04	4.380E-04		3.141E-06	1.133E-05
Pu-241	8.319E-05	9.821E-05	7.934E-05		4.264E-08	2.593E-07
BARC	Core1			Lateral blanket		
Isotope	BOL	Mid Point	EOL	BOL	Mid Point	EOL
U-238	6.360E-03	5.976E-03	5.629E-03	1.037E-02	1.024E-02	1.010E-02
Pu-239	6.072E-04	6.565E-04	6.711E-04		1.247E-04	2.360E-04
Pu-240	2.433E-04	2.604E-04	2.763E-04		1.791E-06	6.594E-6
Pu-241	6.360E-03	5.976E-03	5.629E-03		1.628E-08	1.109E-07
RRC KI	Core1			Lateral blanket		
Isotope	BOL	Mid Point	EOL	BOL	Mid Point	EOL
U-238	6.360E-03	5.969E-03	5.621E-03	1.037E-02	1.023E-02	1.009E-02
Pu-239	6.072E-04	6.604E-04	6.753E-04		1.288E-04	2.417E-04
Pu-240	2.433E-04	2.552E-04	2.663E-04		1.958E-06	6.877E-06
Pu-241	6.360E-03	5.969E-03	5.621E-03		2.197E-08	1.326E-07
TokyoTech	Core1			Lateral blanket		
Isotope	BOL	Mid Point	EOL	BOL	Mid Point	EOL
U-238	6.360E-03	2.650E-02	2.510E-02	1.037E-02	3.124E-02	3.084E-02
Pu-239	6.072E-04	2.488E-03	2.644E-03		3.410E-04	6.500E-04
Pu-240	2.433E-04	9.360E-04	1.009E-03		5.908E-06	2.082E-05
Pu-241	8.319E-05	2.119E-04	1.752E-04		7.309E-08	4.425E-07

Table 19 shows received from the participants evolution of nuclear density of U-238 and Pu isotopes in Core1 and Lateral blanket at 3 points during the cycle – beginning of the life (BOL), Mid point (900 EFPD) and end of life (EOL, 1800 EFPD). Data from ANL and TokyoTech is not valid because of U-238 density at the Mid Point is greater than at the BOL. Data from BARC is similar to data from RRC KI, so similar are evolutions of keff during the cycle.

Table.20 Fission product parameters evolution during the cycle

ANL	Core1		Lateral blanket	
Mid Point, 900 EFPD	$\rho$ , 1/(barn-cm)	$\Sigma a$ , 1/cm	$\rho$ , 1/(barn-cm)	$\Sigma a$ , 1/cm
Rare Earth Lumped	1.69E-04	8.98E-06	7.02E-06	3.88E-07
Other Lumped	1.69E-04	6.04E-05	7.02E-06	2.32E-06
Total	3.38E-04	6.94E-05	1.40E-05	2.71E-06
EOL, 1800 EFPD	$\rho$ , 1/(barn-cm)	$\Sigma a$ , 1/cm	$\rho$ , 1/(barn-cm)	$\Sigma a$ , 1/cm
Rare Earth Lumped	3.36E-04	1.78E-05	1.99E-05	1.08E-06
Other Lumped	3.36E-04	1.20E-04	1.99E-05	6.73E-06
Total	6.72E-04	1.38E-04	3.98E-05	7.81E-06
RRC KI	Core1		Lateral blanket	
Mid Point, 900 EFPD	$\rho$ , 1/(barn-cm)	$\Sigma a$ , 1/cm	$\rho$ , 1/(barn-cm)	$\Sigma a$ , 1/cm
Rare Earth Sum	1.52E-04	3.38E-05	5.39E-06	2.45E-06
Other Fission Products	5.38E-04	1.01E-04	1.83E-05	5.33E-06
Total	6.89E-04	1.35E-04	2.37E-05	7.77E-06
EOL, 1800 EFPD	$\rho$ , 1/(barn-cm)	$\Sigma a$ , 1/cm	$\rho$ , 1/(barn-cm)	$\Sigma a$ , 1/cm
Rare Earth Sum	2.97E-04	6.27E-05	1.54E-05	5.53E-06
Other Fission Products	1.05E-03	1.94E-04	5.32E-05	1.36E-05
Total	1.35E-03	2.56E-04	6.86E-05	1.92E-05
BARC	Core1		Lateral blanket	
Mid Point, 900 EFPD	$\rho$ , 1/(barn-cm)	$\Sigma a$ , 1/cm	$\rho$ , 1/(barn-cm)	$\Sigma a$ , 1/cm
Integrated fission product	6.69E-04		2.38E-05	
EOL, 1800 EFPD	$\rho$ , 1/(barn-cm)	$\Sigma a$ , 1/cm	$\rho$ , 1/(barn-cm)	$\Sigma a$ , 1/cm
Integrated fission product	1.32E-03		6.82E-05	

Table 20 shows received from the participants evolution of fission product parameters in Core1 and Lateral blanket at 3 points during the cycle – beginning of the life (BOL), Mid point (900 EFPD) and end of life (EOL, 1800 EFPD). Total fission product densities and neutron capture rates in ANL simulation are about a half of these parameters in BARC and RRC KI simulations. It seems that fission product capture cross sections used by ANL are correct and fission product nuclear density calculations were incorrect. In any case results of ANL simulation must be revised. BARC and RRC KI simulations of fission product parameters are very close.

Table.21 Main fission product parameters evolution during the cycle

TokyoTech	Core1		Lateral blanket	
Mid Point, 900 EFPD	$\rho$ , 1/(barn-cm)	$\Sigma a$ , 1/cm	$\rho$ , 1/(barn-cm)	$\Sigma a$ , 1/cm
Ru-101	6.66E-05	4.07E-05	2.62E-06	2.27E-06
Rh-103	7.58E-05	8.50E-08	2.57E-06	2.02E-06
Pd-105	5.80E-05	4.79E-05	1.82E-06	2.02E-06
Tc-99	7.40E-05	3.91E-05	2.76E-06	2.02E-06
Pd-107	3.74E-05	3.33E-05	8.36E-07	1.04E-06
Cs-133	7.98E-05	2.98E-05	2.97E-06	1.76E-06
Sm-149	1.34E-05	2.26E-05	6.16E-07	1.78E-06

Other fission products	3.36E-02	3.55E-04	3.17E-02	4.60E-05
Integrated fission products	3.40E-02	5.68E-04	3.17E-02	5.89E-05
Total				
EOL, 1800 EFPD	$\rho$ , 1/(barn·cm)	$\Sigma a$ , 1/cm	$\rho$ , 1/(barn·cm)	$\Sigma a$ , 1/cm
Ru-101	1.25E-04	7.72E-05	6.76E-06	5.87E-06
Rh-103	1.60E-04	9.38E-05	7.22E-06	5.66E-06
Pd-105	1.09E-04	9.07E-05	5.08E-06	5.64E-06
Tc-99	1.49E-04	7.94E-05	7.26E-06	5.32E-06
Pd-107	7.10E-05	6.36E-05	2.57E-06	3.21E-06
Cs-133	1.55E-04	5.83E-05	7.82E-06	4.62E-06
Sm-149	2.31E-05	3.94E-05	1.49E-06	4.29E-06
Other fission products	3.65E-02	5.91E-04	3.19E-02	7.10E-05
Integrated fission products	3.64E-02	1.09E-03	3.19E-02	1.06E-04
Total				
RRC KI	Core1		Lateral blanket	
Mid Point, 900 EFPD	$\rho$ , 1/(barn·cm)	$\Sigma a$ , 1/cm	$\rho$ , 1/(barn·cm)	$\Sigma a$ , 1/cm
Ru-101	2.14E-05	1.24E-05	7.40E-07	6.68E-07
Rh-103	2.05E-05	1.18E-05	6.72E-07	5.87E-07
Pd-105	1.72E-05	1.21E-05	5.16E-07	5.54E-07
Tc-99	1.95E-05	1.00E-05	7.08E-07	5.47E-07
Pd-107	1.03E-05	8.20E-06	2.50E-07	3.09E-07
Cs-133	2.27E-05	7.71E-06	7.93E-07	4.99E-07
Sm-149	3.96E-06	5.61E-06	1.58E-07	5.01E-07
Other fission products	5.74E-04	6.74E-05	1.99E-05	4.11E-06
Integrated fission products				
Total	6.89E-04	1.35E-04	2.37E-05	7.77E-06
EOL, 1800 EFPD	$\rho$ , 1/(barn·cm)	$\Sigma a$ , 1/cm	$\rho$ , 1/(barn·cm)	$\Sigma a$ , 1/cm
Ru-101	3.99E-05	2.29E-05	2.15E-06	1.71E-06
Rh-103	4.00E-05	2.29E-05	2.06E-06	1.61E-06
Pd-105	3.20E-05	2.22E-05	1.56E-06	1.48E-06
Tc-99	3.66E-05	1.87E-05	2.03E-06	1.40E-06
Pd-107	1.91E-05	1.51E-05	8.08E-07	8.69E-07
Cs-133	4.35E-05	1.45E-05	2.30E-06	1.20E-06
Sm-149	6.94E-06	9.66E-06	4.33E-07	1.04E-06
Other fission products	1.13E-03	1.31E-04	6.82E-05	1.81E-05
Integrated fission products				
Total	1.35E-03	2.56E-04	6.86E-05	1.92E-05

Table 21 shows evolution of main fission product parameters in Core1 and Lateral blanket at 3 points during the cycle – beginning of the life (BOL), Mid point (900 EFPD) and end of life (EOL, 1800 EFPD) in simulations performed by TokyoTech and RRC KI. Data from TokyoTech are something strange, especially in lines “Other fission products” and “Integrated fission products”. In any case results of TokyoTech simulation must be revised.

## Conclusion

1. Neutron multiplication factor depends on data library used and discrepancy can be more than 1.5 %  $\Delta(1/k)$  (~1900 pcm). That is about 2 times larger than discrepancies in  $k_{eff}$  at the beginning of life.
2. Multigroup neutron cross section libraries generated using neutron spectra different from benchmark ones are the source of additional discrepancies in neutron multiplication factor. For example, in all multigroup calculations for U-238 total fission neutron production is adopted ~2.7 whereas MCNP5 calculations result is ~2.5.
3. At this stage of investigations we cannot define the effect of Pb inelastic cross section uncertainties on the benchmark reactivity.
4. All participants can calculate correct region power distributions during the cycle. Evolution of  $k_{eff}$  on 1800-day campaign in BARC, Gidropress, RRC KI and TokyoTech simulations are the same type – slight increase due to breeding in blankets and then decrease due to fission products accumulation. ANL simulation, however, presents  $k_{eff}$  growing during the cycle. The reason is that neutron capture by fission products is about half of value of this component in other simulations.
5. Evolution of U-238 and Pu isotopes nuclear density from BARC is similar to data from RRC KI. Also evolution of fission product total density and neutron capture rate is very similar in both simulations. So evolutions of  $k_{eff}$  during the cycle are similar.
6. Taking into account the different nuclear data libraries the results of the RBEC-M benchmark simulation performed by BARC and RRC KI are very close. Results of ANL and TokyoTech simulations in any case are not valid and must be revised.

## References

1. “Энциклопедия нейтронных данных РОСФОНД (Российская библиотека файлов оцененных нейтронных данных). Полный пакет обоснований отбора оценок”. Федеральное агентство Российской Федерации по атомной энергии, Федеральное государственное унитарное предприятие Государственный Научный Центр Российской Федерации Физико-энергетический институт им. А.И.Лейпунского. Обнинск, 2006.
- 2 Smirnov V., Orlov V., Mourogov A., Lecarpentier D., Ivanova T., “The lead cooled fast reactor benchmark BREST-300: analysis with sensitivity method”. *Mathematics and Computation, Supercomputing, Reactor Physics and Nuclear and Biological Applications*. Palais des Papes, Avignon, France, September 12-15, 2005, on CD ROM, American Nuclear Society, LaGrange Park, IL, (2005).
3. Milošević M., Greenspan E., Vujić J., “Effects of uncertainties in lead cross section data in Monte Carlo analysis of lead cooled and reflected reactors”. *Joint International Topical Meeting on Mathematics & Computation and Supercomputing in Nuclear Applications (M&C + SNA 2007)*. Monterey, California, April 15-19, 2007, on CD-ROM, American Nuclear Society, LaGrange Park, IL, (2007).

## Appendix 1. ANL Analysis Method

The ANL suite of fast reactor analysis codes was used to analyze the RBEC benchmark problem. Detailed fuel cycle analysis was performed using the DIF3D/REBUS-3 code system. Multi-group cross section data was generated for each homogenized zone in the benchmark using the MC<sup>2</sup>-2 code based upon ENDF/B-V.2 data. The flux calculations were performed using the discrete ordinate transport code TWODANT with comparative results generated using the DIF3D finite difference diffusion theory option (DIF3D-FD).

For each of the 15 homogenized physical zones, 33-group and 230-group cross section structures were implemented for the specified composition and component-wise temperatures using the MC<sup>2</sup>-2 code. ENDF/B-V.2 data was used for all isotopes. For the three core zones, a critical buckling calculation was used with a consistent P<sub>1</sub> approximation and the corresponding spectrum was used for group collapsing. For the remaining compositions, a fixed source, derived from the leakage spectrum from an adjacent zone, was used to determine the collapsing spectrum. As an example, the leakage spectrum from the core zone was used as a fixed source in the adjoining blanket region to obtain a new collapsing spectrum. The leakage spectrum derived from the blanket calculation was then used as a fixed source in the fission gas plenum. This process is replicated for all other regions progressing the leakage from the core through all adjoining regions in the domain.

For resolved resonance integral calculation, the narrow resonance approximation was used, and the Doppler broadening, interference scattering, and the effects of overlap with neighboring resolved resonances were taken into account. It is noteworthy that an additional option is available to use the hyper-fine group integral transport calculation with RABANL, in which the Doppler width is divided into a few hyper-fine groups. In the preparation of MC<sup>2</sup>-2 library, wide and extremely weak resonances are pre-processed and represented by the ultra-fine-group (2082 group) energy structure of MC<sup>2</sup>-2. The other resonances are modeled by their resonance parameters, and their self-shielding effects are explicitly evaluated in the MC<sup>2</sup>-2 calculation. The unresolved resonance integral calculation was performed with a narrow resonance approximation, and interference scattering, the effects of overlap with resonances in other spin sequences, and the effects of self-overlap with resonances of the same spin sequences were taken into account. The resolved and unresolved energy range used is specified by the ENDF data and is unique for each nuclide. The (n,2n) reaction was treated as a source term in the ultra-fine-group spectrum calculation. For the secondary energy distribution, tabulated function, evaporation spectrum and discrete levels were used. The discrete ultra-fine-group (n,2n) scattering source was approximately treated by neglecting the energy-angle correlation.

The flux distributions were mainly computed using the TWODANT transport theory code using the 33-group cross section set unless otherwise specified. An R-Z computational model was employed in these calculations with ~2.0 cm mesh size. For comparison, the finite difference diffusion theory option of the DIF3D was also used. It is noted that the DIF3D code is a collection of modules that provide various solution options for eigenvalue and fixed source problems: variation nodal transport (VARIANT), nodal diffusion theory, and finite difference diffusion theory options. The power distributions were not obtained along the discrete lines specified but instead derived from mesh centered quantities. As an example, the first radial mesh was 2.39 cm wide. The power

was calculated for the series of meshes from the bottom of the core to the top within this first mesh and thus belongs to the volume associated with a 2.39 cm wide strip. A similar approach was taken for the radial power distributions where the mesh size was 2.5 cm in both cases.

The fuel cycle analyses were performed using the REBUS-3 code, which was developed for fast reactor depletion and fuel cycle analysis. Both the core and blanket zones were represented by five axial depletion regions. The region density iteration was performed with a relative convergence criterion of 0.0005 on calculated material densities. That is, the depletion calculation for each region was performed with the average of the beginning and end of time interval fluxes. The end of time interval flux was iteratively computed by iteration on the final nuclide densities. The depletion calculations were performed using burnup chains for nuclides ranging from U-234 to Cm-246. Capture, (n,2n), and fission reactions were considered for all actinide isotopes included in the burn chains. In the capture and (n,2n) reactions, short-lived intermediate products were neglected. As a result, the products of capture reactions of U-238, Np-238, Pu-242, and Am-243 were represented by Pu-239, Pu-239, Am-243, and Cm-244, respectively. The capture reaction of Am-241 was modeled to yield Cm-242, Am-242m, and Pu-242 with yield fractions of 0.66, 0.20, and 0.14, respectively. The products of (n,2n) reactions of Pu-238 and Am-241 were respectively represented by Np-237 and Pu-240. The (n,2n) reaction of Am-243 was assumed to yield Am-242m, Pu-242, and Cm-242 with yield fractions of 0.5, 0.086, and 0.414, respectively. Cm-242 was assumed to yield Am-241 in 99% of its (n,2n) reactions and Np-237 in 1%. It was assumed that 37.4% of (n,2n) reactions of Np-237 yield U-236 and the remaining 62.6% yield a fictitious dummy isotope. The end products of Cm-246 capture and U-234 (n,2n) reactions were represented by a fictitious dummy isotope. Important  $\alpha$  and  $\beta$  decays of actinide isotopes were also considered. Specifically,  $\alpha$  decay was considered for all actinide isotopes except for Np-238 and Pu-241. The  $\beta^-$  decays of Np-238, Pu-241, Am-242m and the  $\beta^+$  decay of Am-242m were also included in the burn chains. The employed decay constants for the  $\beta^-$ ,  $\beta^+$ , and  $\alpha$  decays of Am-242m were 1.189E-10, 2.487E-11, and 7.225E-13, respectively. The fission products were modeled with five lumped rare earth elements and five lumped fission products. The cross sections of these lumped elements were generated by weighting the cross sections of 180 fission products with fission yields of U-235, U-238, Pu-239, Pu-240, and Pu-241, respectively. Three dummy isotopes were also used to represent the other end products not included in the chains. For full reactor depletion calculations, the lumped fission products of U-234, U-235, and U-236 were represent by those of U-235, while the fission products of U-237, U-238, Np-237, Np-238, and Pu-238 were represented by those of FP38. The fission products of Pu-241 and higher actinides were represented by those of Pu-241.

A 100-day depletion time interval was used for all calculations. For Mode 3, two options of the REBUS-3 module were used. The first follows the approach described in the benchmark where 1/6 of the core material is replaced with fresh fuel during each shutdown phase. That is, 1/6 of each of once-burned to six-cycle-burned fuels is replaced with fresh fuel. The second utilizes the equilibrium cycle option of REBUS-3 where the six-cycle burned fuel is replaced with fresh fuel. At the sixth cycle, the Mode 3 calculation very closely resembles that of the equilibrium cycle mode. It is important to note however, that if one continues the approach used in Mode 3 for additional fuel cycles that this trend will not continue. This is due to the fact that there will be fuel material in the core for more than six cycles.

We performed the calculation using transport corrected P0 cross sections derived from ENDF-V.2 cross section data in the diffusion theory solver DIF3D with 3, 9, and 18 time steps (300 day, 100 day, and 50 day). We also performed the calculation using P1 anisotropic cross section data again derived from ENDF/B-V.2 in the TWODANT solver with a  $S_8$  level symmetric even-moment cubature. In all of the following, the results are taken from the TWODANT calculations.

In both cases we utilize a finite difference spatial discretization with an average spatial mesh size of 2.5 cm in both the radial and axial directions. We performed calculations to ascertain the combined space-angle discretization error is sufficiently small and concluded that a 2.5 cm mesh size combined with a  $S_8$  angular approximation was sufficiently converged.

Description in detail the sequence of steps in depleting the number densities in all regions including:

- How finely the region is subdivided
  - We split the inner core or Core 1 region into three radial depletion zones and five axial depletion zones (28 cm radial and 20 cm axial).
  - We split the middle core or Core 2 region into two radial depletion zones and five axial depletion zones (23 cm radial and 20 cm axial).
  - We split the outer core or Core 3 region into one radial depletion zone and five axial depletion zones (17 cm radial and 20 cm axial).
  - We split the axial blanket of core-1 into three radial depletion zones and one axial depletion zone (28 cm radial and 10 cm axial).
  - We split the axial blanket of core-2 into two radial depletion zones and one axial depletion zones (23 cm radial and 10 cm axial).
  - We split the axial blanket of core-3 into one radial depletion zone and one axial depletion zones (17 cm radial and 10 cm axial).
  - We split the lateral blanket into seven axial regions and one radial region (10, 20, 20, 20, 20, and 10 cm).
- How the flux is normalized
  - The fission power is computed using standard ENDF/B-V.2 isotope dependent conversion factors. Gamma heating is also accounted for by combining the  $(n,\gamma)$  reaction cross section and the “heat deposition factors.” This approach assumes the gamma ray energy is deposited locally where the  $(n,\gamma)$  interaction occurs. We can estimate the total fraction of power by capture as 0.04.
- Whether the isotopes are depleted by group fluxes or by a one-group flux
  - We implemented a 33 group cross section set and the 33 group flux solution in addition to a 230 group cross section set and a 230 group flux solution to perform the depletion (two separate calculations).
  - In all calculations we utilized two lumped fission products (rare earths are separated out for one of the products) for each of the major fissionable actinides U-235, U-238, Pu-239, Pu-240, and Pu-241.

## Appendix 2. BARC Analysis Method

The European reactor analysis code package ERANOS2.0 was employed to simulate the benchmark at BARC.

The JEF2 nuclear data libraries supplied with the code package are used. The JEF2 libraries have adjusted nuclear data values for the main nuclei. The burnup is done at the core level with 6 pseudo fission products. The number of energy groups used for the core calculations are 33. The burnup is computed in the following way. For a starting nuclides concentration  $N_0$ , and using a constant value over burnable zones for flux and cross sections,

$$N(t) = \exp(\mathbf{M}t) N_0, \quad \mathbf{M} = \Phi \mathbf{R} + \mathbf{D}$$

Where  $\mathbf{R}$  is cross section matrix and  $\mathbf{D}$  is decay matrix.

In the RZ geometry, the code ERANOS considers each radial and axial zone as burnable zone. Further sub-divisions are possible in axial zones by the Burnable\_Zone directive which is not used in these calculations. The flux is normalized to the total power produced in the reactor including blanket and isotopes are depleted by one-group fluxes.

### Appendix 3. RRC KI Analysis Method

In RRC KI suite of neutron-physical codes was used to analyze the benchmark problems. Criticality calculations were performed with the MCNP5 Monte Carlo code. Neutron data for MCNP5 were obtained using code system NJOY99 (version 99.90) from libraries of evaluated nuclear data files ENDF/B, JEFF and JENDL. For each nuclide the set of data for required temperatures was generated with tolerance 0.005.

The fuel cycle analyses were performed using the ISTAR-2 code system developed for analysis of fuel cycles of multi-component nuclear power systems with advanced reactors. Code system has abilities to perform equilibrium or non-equilibrium cycle calculations for the set of processes – reactors, reactor zones, cooling, reprocessing (with or without neutron flux) – and nuclide streams between them. The radioactive decay is also taken into account.

Non-equilibrium cycle analyses were performed for the benchmark problems. Each of core and blanket zones was represented as a single depletion zone. In each depletion zone the isotope kinetics problem was solved for united vector of heavy nuclides and fission products.

The volume averaged neutron cross-sections were obtained and transported to electronic table from the criticality calculations with the MCNP5 code – for heavy nuclides  $\sigma(n, \gamma)$ ,  $\sigma(n, \text{fission})$ ,  $\sigma(n, 2n)$ ,  $\sigma(n, 3n)$ ,  $\sigma(n, n'+\alpha)$ ,  $v_{\text{total}}$ ; and for fission products  $\sigma(n, \gamma)$ .

Parameters for radioactive nuclides decay –  $\alpha$ ,  $\beta^-$ ,  $\beta^+ + n$ ,  $\beta^-$  with daughter nuclide in 1<sup>st</sup> excited state,  $\beta^+$  or EC, isomer transition from 1<sup>st</sup> excited state to ground state, isomer transition from 2<sup>nd</sup> excited state to 1<sup>st</sup> excited state, spontaneous fission – were obtained and transported to electronic table from ENDF/B-6 decay data library and Table of Isotopes CD ROM. In general, any other decay type can be included into electronic table.

Parameters for fission products generation were obtained from ENDF/B-6 fission product yield sublibraries. Special investigations were performed to reduce the size of fission products yield vector from 1325 to 1098, and data for seven nuclides from JENDL-3.2 library was added, thus the resulting nuclide of decay or  $(n, \gamma)$  reaction belongs to the same fission products vector.

Energy per fission for certain actinides were recommended by Monteburns 2.0 manual. For others 200 MeV per fission is adopted.

Probability of Np-236m production in Np-237(n, 2n) reaction averaged by reactor core spectrum is adopted 0.644.

Probability of Am-242m production in Am-241(n,  $\gamma$ ) reaction averaged by reactor core spectrum is adopted 0.25.

With this data code system ISTAR-2 generates the matrix of isotope kinetics problem and uses LSODES code to solve this problem for given burnup interval.

To increase the accuracy of the burnup calculations the standard “mid-step” methodic was used. With the MCNP5 code for each region (cores and blankets) volume averaged one-group cross-sections for heavy nuclides and fission products were calculated. In the same calculation the contribution of each region to fission (thermal) power was obtained. Then the beginning of time step (BOTS) neutron fluxes were computed in the assumption that the cross-sections don't change during burnup step and region energy production during time step corresponds to region power at the BOTS. With this data isotope kinetics problem was solved for region and end of time step (EOTS) nuclear densities was obtained. With MCNP5 code EOTS thermal power of region was calculated and mid-step region power was obtained and mid-step neutron flux was computed. Then isotope

kinetics problem once more was solved for region and final EOTS nuclear densities were obtained. This procedure was used for next time step and so on.

In the Mode.1 and Mode.2 calculations the employed burnup interval was 900 days for the first and second problems. At the BOTS volume averaged one-group cross-sections for all nuclides were recalculated. Some calculations show that cross-sections vary slowly during 100 day burnup, so 200-days and 300-days burnup intervals can be used in the later analysis.

## Appendix 4. TokyoTech Analysis Method

Depletion calculation is performed in each mesh. In the calculation, Runge-Kutta method is used for solving following depletion equation.

$$\frac{dN_i}{dt} = -\lambda_i N_i - \sum_g \sigma_{a,i} \phi_g N_i + \sum_{j,g} \lambda_{g,j} \alpha_{j \rightarrow i} N_j + \sum_{j,g} \beta_{j \rightarrow i} \sigma_{a,g,j} \phi_g N_j + \sum_{j,g} \gamma_{j \rightarrow i} \sigma_{f,g,j} \phi_g N_j$$

Microscopic cross sections of each nuclides and energy groups are calculated by SRAC code system that is produced by JAEA (Japan Atomic Energy Agency). In this system, JENDL-3.3 is used as nuclear data set. These cross sections are not renewed and used till the end of all calculation. Neutron flux which is used in depletion calculation is calculated in the previous diffusion calculation. This is normalized by total power (900MWt). Burn-up chain and FP yield data are taken from JENDL-3.3.

After the above calculation, macroscopic cross section is calculated by nuclide number densities from depletion calculation and microscopic cross sections of each group. This value is used in next diffusion calculation.